Computation on shape manifold for atlas generation: application to whole heart segmentation of cardiac MRI

Xiahai Zhuang[a], Wenzhe Shi[b], Haiyan Wang[b], Daniel Rueckert[b], Sebastien Ourselin[c]

[a]Shanghai Advanced Research Institute, Chinese Academy of Sciences, China
[b]Biomedical Image Analysis Group, Imperial College London, UK
[c]Centre for Medical Image Computing, University College London, UK

ABSTRACT

In this work, we investigate the computation on a shape manifold for atlas generation and application to atlas propagation and segmentation. We formulate the computation of Fréchet mean via the constant velocity fields and Log-Euclidean framework for Nadaraya-Watson kernel regression modeling. In this formulation, we directly compute the Fréchet mean of shapes via fast vectorial operations on the velocity fields. By using image similarity metric to estimate the distance of shapes in the assumed manifold, we can estimate a close shape of an unseen image using Naderaya-Watson kernel regression function. We applied this estimation to generate subject-specific atlases for whole heart segmentation of MRI data. The segmentation results on clinical data demonstrated an improved performance compared to existing methods, thanks to the usage of subject-specific atlases which had more similar shapes to the unseen images.

Keywords: Shape, Manifold, Atlas Generation, Segmentation, Whole Heart Segmentation, Cardiac MRI

1. INTRODUCTION

Computation on shape manifolds is useful for population based studies such as regression modeling[1,2] and manifold learning.[3–5] To better represent the natural variability of shapes, many works proposed to employ the computation of statistics on a Riemannian manifold, instead of on the Euclidean vector space for the study of shapes and images.[1,3,6,7] In this setting, the distance metric can be naturally defined to the geodesic distance in the manifold and the statistics computation is generally achieved by iterative optimization schemes.

The computation on diffeomorphisms can be converted to simple and efficient computation of velocity vectors on the Euclidean vector space via the Log-Euclidean framework[6] or the DARTEL framework assuming a constant velocity field.[8] In the setting, a diffeomorphic transformation between two coordinates, on which two shapes are defined, is mapped to a velocity vector field, and then the distance metric between two diffeomorphisms can be defined to the Euclidean distance of the two corresponding velocity vectors. This formulation provides a mechanism for fast computation of Fréchet mean or expectation of diffeomorphisms, which can potentially lead to an easy implementation of the Nadaraya-Watson kernel regression function for regression modeling and manifold learning studies.[1,3]

Motivated by this idea, in this paper we first propose a formulation for fast computation of the Fréchet mean on a shape manifold. In this formulation, we parameterize the shape of an image using a diffeomorphic coordinate transformation between the studied image and the reference image. The advantage of this parametrization is that it provides the mechanism to study variations of shapes via the computation on diffeomorphic deformation fields, which has been the focus of several works in the literature such as.[1,6,7] Then, we propose a framework to estimate the shape of an unseen image using the Nadaraya-Watson kernel regression function, where the kernel function is defined in relation to image similarity measures.

For demonstration, we employ the computation on shape manifold and shape estimation for atlas generation and apply the generated atlases for atlas propagation based whole heart segmentation of cardiac MRI. In cardiac MRI, the major challenge of automated segmentation comes from the large shape variability of the heart. Locally

---

Further author information: (Send correspondence to Xiahai Zhuang)
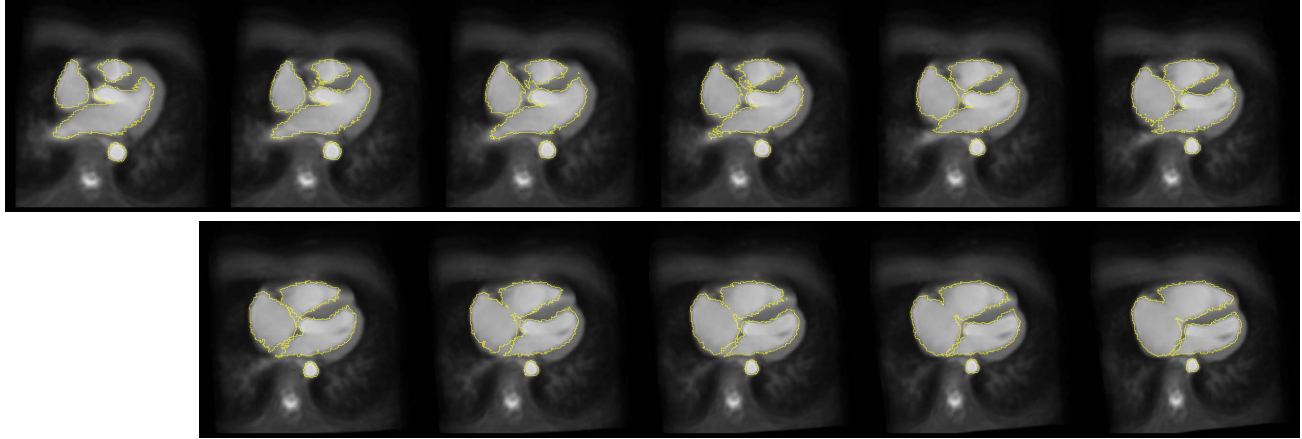Xiahai Zhuang: E-mail: zhuangxh@sari.ac.cn, Telephone: 86 21 2030 5896

Figure 1. Fréchet mean of two cardiac shapes using different weighting scheme, $w \in 0 : 0.1 : 1$ for one and $(1 - w)$ for the other; the most top left is a hypertrophic cardiomyopathy (HCM) case (left ventricle hypertrophy) while the most bottom right is a right ventricle hypertrophy case. They yellow contour line indicates the endocardial surface.

affine registration method was proposed to deal with the large shape variations of the heart across different pathologies.[9] It was also shown in[10] that the closer the shape of the atlas was initialized to the unseen image, the better the segmentation result could be. Therefore, we propose to estimate the shape of an unseen image and generate the corresponding atlases for atlas propagation and segmentation. This estimation is computed from the Fréchet mean of a set of training data. Fig. 1 demonstrates an example where the new atlases are generated from two training images. The generated atlases are expected to have closer shapes to the unseen image than any one from the available training data set, and therefore better segmentation results are expected using the generated atlases compared to directly using the training atlases.

The rest of the paper is organized as follows. We first present the methodology in Section 2, then provide the detail of experiment and results in Section 3, and finally draw the conclusion and discuss the potential future work in Section 4.

2. METHOD

In this section, we first describe representation of shapes and computation of Fréchet mean on a shape manifold; then, we define the distance of shapes using the Log-Euclidean framework, where the computation of Fréchet mean and Nadaraya-Watson kernel regression function can be fast computed; finally we describe the shape estimation and atlas generation techniques.

2.1 Shape and Fréchet mean

We formulate the shape of an image I using a transformation T which registers the local coordinates of I to that of the reference image I_r:

$$\text{Shape}(I) \equiv \underset{T}{\arg} \text{ REG } (I, I_r, T) . \tag{1}$$

Given a set of N images, with associated transformations $\{T_i, i = 1 \ldots N\}$, the general weighted Fréchet mean of the transformations is given by:[1,3]

$$m(\{T_i\}) = \underset{T}{\arg\min} \sum_{i}^{N} w_i \times dist(T_i, T)^2 , \tag{2}$$

where $dist(T_i, T)$ is the distance between two shapes on an assumed manifold and $w_i = 1/N$ if the same weight is used for all observations. For example, by assuming transformation T on the pEuclidean vector space, the distance metric is then defined as the Euclidean distance, $dist(T_i, T) \equiv ||T_i - T||_2$. However, a number of works proposed that shapes of images should be studied on a Riemannian manifold, a manifold of diffeomorphisms, to better represent the natural variability of shapes.[1,3,6,11,12] Therefore, a diffeomorphic deformation between two images is used to define the distance between the two shapes.

2.2 Distance on shape manifold

The Lagrangian ordinary differential equation (ODE) can be used to estimate a solution for a diffeomorphic transformation between the coordinates on which the studied images or shapes lie:

$$\frac{d}{ds}\phi_s(x) = v_s(x) , \tag{3}$$

where $s \in [0,1]$ is the time parameter, ϕ_s and v_s are displacement and velocity vectors respectively, and $T(x) = x + \phi_s(x)$. To represent the geodesic distance between two shapes, a constraint which penalizes the integrated distance of the flow is applied to the registration of the two images:

$$\text{REG } (I, I_r, T) \equiv \arg\max_T \text{SIM}(I, I_r, T) , \text{ subject to } \min_v \int_0^1 ||v_s(x)||_L^2 , \tag{4}$$

where SIM is the similarity metric and operator L can be defined in relation to magnitude and derivatives of v_s.[7,13]

Given two images, I_1 and I_2, and their associated deformations T_1 and T_2 computed from the registration to reference image I_r using (4), the distance between the two shapes is defined to the distance of T_1 and T_2 on the diffeomorphism manifold:

$$dist(\text{Shape}(I_1), \text{Shape}(I_2)) \equiv dist(T_1, T_2) . \tag{5}$$

2.3 Log-Euclidean formulation for computation of constant velocity

In,[6,8] the constant velocity (flow) field is assumed for the diffeomorphic registration. Given T which is a resultant deformation of registration formulated in (4) and represents the shape of image I in a reference coordinate of I_r, we can estimate the corresponding constant velocity v using the Log-Euclidean framework as follows:

$$v(x) = \log \phi(x) = \log(T - Id)(x) . \tag{6}$$

Similarly, the transformation T can be recovered from the constant velocity v using $T(x) = x + \exp(v(x))$. The computation of logarithms can be estimated using the scaling and square rooting steps, while the computation of exponentials can be fast estimated using the scaling and squaring steps.[6] In the cardiac MRI experiment in Section 3, the computation of logarithms takes about one hour, while the computation of exponentials only takes a few seconds.

The advantage of using constant velocity field representation for shapes is that it provides a well defined *distance metric* between two diffeomorphisms via a Euclidean norm, e.g. the second order norm $|| \cdot ||_2$, on velocity vectors:

$$dist(T_1, T_2) = || \log(\phi_1) - \log(\phi_2) ||_2 = ||v_1 - v_2||_2 . \tag{7}$$

It should be noted that this computation does not guarantee a geodesic distance on the shape manifold $\mathcal{M}$, instead it is on the local tangent space of $\mathcal{M}$ near the identity. However, this metric, (7), can be efficiently computed compared to traditional computation of geodesics, and it satisfies the definition of distance and thus is well defined.

Motivated by this definition of distance metric for shapes in (7), we then extend the computation of Fréchet mean in (2) as follows:

$$m(\{T_i\}) \equiv x + \exp(\bar{v}) , \tag{8}$$

where,

$$\bar{v} = \arg\min_v \sum_i^N w_i ||v_i - v||^2 \text{ and } v_i = \log \phi_i . \tag{9}$$

Because the velocity vectors $\{v_i\}$ are on Euclidean vector space, the Fréchet mean of them can be directly computed usingp $\bar{v} = \sum_i^N w_i v_i$. Hence, the Fréchet mean (sum) of shapes is then given by:
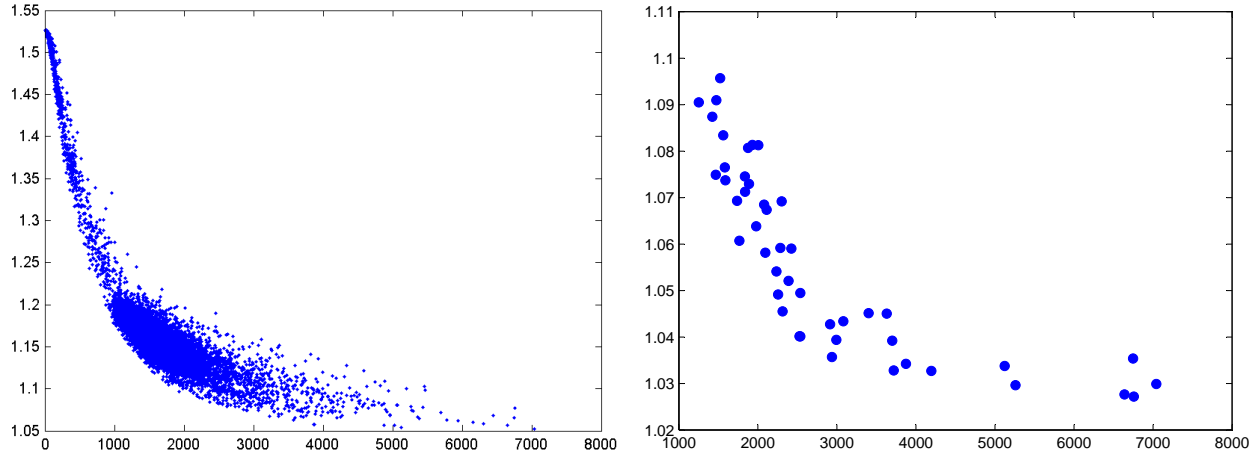
$$m(\{T_i\}) \equiv x + \exp(\sum_i^N w_i v_i) . \tag{10}$$

Figure 2. NMI values against distance of transformations ($dist(Id, T)$). Left: NMI is computed between atlas intensity image I_A and transformed atlas image $T(I_A)$,[10] T is computed using (10) where $\{w_i\}$ are random values from [0,1] and $\{v_i\}$ are computed from training shapes. Right: NMI is computed between I_A and test images.

Fig. 1 illustrates a set of generated shapes from two shapes (the most top left and the most bottom right) using different weights.

Similarly, the Nadaraya-Watson kernel regression function for shapes in,[1,3]

$$m_k = \operatorname*{arg\,min}_{T \in \mathcal{M}} \frac{\sum_{i=1}^{N} K_h(t - t_i) dist(T, T_i)^2}{\sum_{i=1}^{N} K_h(t - t_i)}, \tag{11}$$

can be computed in the proposed formulation, using (10), as follows:

$$m_k \equiv x + \exp\left(\sum_i^N w_i v_i\right) \text{ and } w_i = \frac{K_h(t - t_i)}{\sum_{i=1}^{N} K_h(t - t_i)}, \tag{12}$$

where $K_h(t)$ is a kernel function which satisfies $\int_R K(t) dt = 1$.

2.4 Estimating shape for atlas generation

For illustration, we apply the computation on the cardiac shape manifold to generate new atlases for atlas propagation based whole heart segmentation. Given a cardiac atlas which consists of an intensity image I_A and a label image I_A, in theory we can register the atlas intensity image to any unseen image for segmentation propagation.[9] However, it has been shown in both single propagation[9] and multiple propagation and segmentation[10] that using an atlas, which has a similar heart shape to the unseen image, has the potential to achieve better results for cardiac MRI. Therefore, we propose to generate new atlases which have more similar shapes to unseen images for atlas propagation and segmentation.

Let I_A be an atlas intensity image as the reference image and $\{I_i\}$ be a set of training images. The shapes of $\{I_i\}$ are defined by the coordinate transformations $\{T_i\}$ computed from the registration between the atlas and training images. For an unseen image I_u, we propose to estimate the shape of I_u using the Nadaraya-Watson kernel regression model in (12). The variable t in the kernel function is defined to the distance between the two shapes of the atlas and unseen image, $t = dist(Id, T_u)$, where Id is identity and T_u is the coordinate transformation between I_A and I_u. However, T_u is unknown before the propagation registration. Image similarity measures are commonly used to estimate the distance between two images, as Fig. 2 shows the relation between normalized mutual information (NMI) of cardiac MRI images[10] and the transformation distance. Furthermore, we also need to define the kernel function K_h in order to compute (12). Therefore, we define $K_h(dist(Id, T_u))$ using NMI, as follows:

$$K_h(dist(Id, T_u)) = \begin{cases} a(\text{NMI}(I_A, I_u) - b), & \text{if } \text{NMI}(I_A, I_u) - b > \epsilon \\ 0, & \text{otherwise} \end{cases} \tag{13}$$
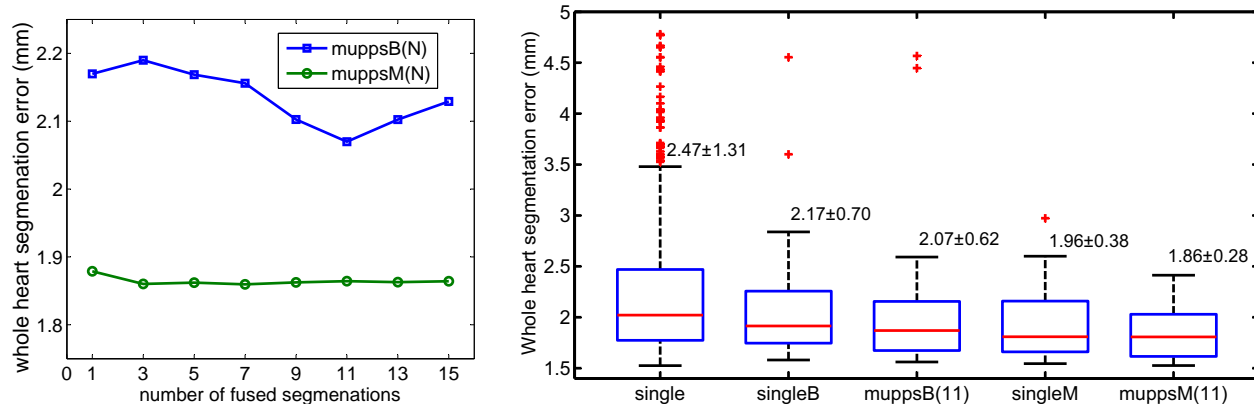
Figure 3. Left: root mean square surface distance of whole heart segmentation error by **muppsB**(N) and **muppsM**(N) with respect to number of fused segmentations. Right: box plots of whole heart segment errors by the five segmentation methods and the mean and standard deviation of each group.

where a will disappear when plugging (13) into (12), b can be estimated from training data as follows:

$$b = \min \left\{ \text{NMI}(T_i(I_A), I_u) \right\}, i = 1 \ldots N, \tag{14}$$

and $\epsilon \geq 0$ is a user-defined value to exclude these samples which are far away from I_u.

Using (12) and (13), we can estimate a shape, transformation $\hat{T}_u$, for the unseen image I_u, and generate a new atlas, $\hat{T}_u(I_A)$, which has similar shape to I_u for segmentation propagation.

3. EXPERIMENT

We employed 24 *in vivo* cardiac MRI data, $\{I_i\}$, among which 19 were from different pathologies (myocardium infarction, atrial fibrillation, tricuspid regurgitation, aortic valve stenosis, aortic coarctation, Alagille syndrome, Williams syndrome, HCM, and Tetralogy of Fallot) and 5 were from healthy volunteers. Each of these images has a manually labeled (segmentation) image on four chambers and great vessels, $\{L_i\}$. To compare with existing methods,[9, 10] we constructed the reference atlas using another set of 10 volunteer data. The atlas intensity image, I_A, was the mean intensity of the 10 registered cardiac MRI images and the label image, L_A, was defined on the mean shape of them.[9] The atlas hence did not have any statistical information of either shapes or intensity distributions. The shapes of the 24 test images were defined by the transformations $\{T_i\}$ which were accurately computed from the registration between L_i and L_A. Logarithms were applied to these transformations to compute the velocity fields $\{v_i\}$. For experiment, we employed leave-one-out strategy by considering one of the test images as the unseen image and the others as the training shapes. For each unseen image, we employed five segmentation methods:

- **single**: use $(T_i(I_A), T_i(L_A))$, $i = 0, 1, \ldots, 23$, as an atlas for single propagation,[9] where T_0 is the identity transformation;
- **singleB**: use $(T_B(I_A), T_B(L_A))$ as an atlas for single propagation where $T_B = \max_{T_i} \text{NMI}(T_i(I_A), I_u)$ using the global affine registration ranking;[10]
- **singleM**: use $(T_M(I_A), T_M(L_A))$ as an atlas for single propagation where T_M is the estimated shape of the unseen image using (12) and (13);
- **muppsB**(N): use $\{(T_b(I_A), T_b(L_A))\}$, $b = 1, \ldots, N$ as the atlas pool for applying the multiple propagation strategy in[10] where $\{T_b\}$ are the transformations which provide the best NMI values among all training shapes;
- **muppsM**(N): randomly select 15 cases from all available training shapes and use them to estimate the shape, T_{M_1}, of the unseen image. This process is repeated N times, resulting in N shapes and atlases, $\{(T_{M_i}(I_A), T_{M_i}(L_A))\}$, $i = 1, \ldots, N$ for multiple propagation.

Both **muppsB**(N) and **muppsM**(N) used the majority voting scheme to fuse the multiple segmentations into one result.[14] The segmentation error was defined to the root mean square distance between the segmented whole heart surface and the gold standard, including endocardium of the four chambers and epicardium of the left ventricle.[9]

Fig. 3 provides the results. Fig. 3 (left) shows that **muppsB**(N) achieved the best performance when 11 best atlases (N=11) was used for propagation and fusion. Also, the segmentation using generated atlases, **muppsM**(N), was always better than **muppsB**(N) regardless the number of fused segmentations. The gain from fusion of multiple segmentations, from 2.17 ± 0.70 to 2.07 ± 0.62 (mm), was evident; while for **muppsM**(N), whose segmentation accuracy was always better than **muppsB**(N) regardless the number of propagations, the gain was smaller. Fig. 3 (right) presents box plots of whole heart segment errors where N=11 was used for **muppsB** and **muppsM**. The mean and standard deviation of the five segmentation results were 2.47 ± 1.31, 2.17 ± 0.70, 2.07 ± 0.62, 1.96 ± 0.38 and 1.86 ± 0.28 (mm) respectively. The segmentation using generated atlases demonstrated better robustness, as it had smaller standard deviation and less outliers in the box plots. This is also confirmed in Fig. 3 (right): compared to **muppsB**(11), **singleM** not only had smaller mean error (1.96 vs 2.07 mm), but also had smaller standard deviation (0.38 vs 0.62 mm) and less outliers in the box plots, which indicates a better robustness. Finally, using the multiple propagation strategy **muppsM**(11) further improved the segmentation from 1.96 ± 0.38 (by **singleM**) to 1.86 ± 0.28 mm.

4. CONCLUSION AND DISCUSSION

In this work, we have presented a new formulation for computing the Fréchet mean on a shape manifold. In this formulation, the distance metric is defined on the constant velocity fields of the coordinate transformations. The transformations define the shapes of images and their corresponding velocity fields lie on a Euclidean vector space. Therefore, the Fréchet mean and Nadaraya-Watson kernel regression model of shapes can be directly and fast computed using vectorial operations on the velocity vectors. We further proposed a method to estimate the shape of an unseen image using the Nadaray-Watson regression function, where the kernel function was defined in relation to the similarity metric between images. We employed this shape estimation for atlas generation and applied to the atlas propagation based whole heart segmentation of cardiac MRI, where the generated atlases had more similar shapes to the unseen images. We compared the segmentation performance from both single and multiple propagations with existing segmentation schemes which employed atlases directly from a training dataset. The experimental results on cardiac MRI showed that even using single one atlas, the proposed segmentation method still achieved better accuracy and robustness than the multiple propagation method in,[10] in particular for the challenging cases where the shapes could differ significantly from any available atlas. Furthermore, the segmentation performance was further improved by combining the atlas generation technique with the multiple propagation strategy.

The proposed computation of Fréchet mean on a shape manifold is generally applicable to other population studies such as regression modeling on brain images[1] where the Nadaray-Watson kernel regression function can be efficiently computed using (12), given the constant velocity fields are computed. For the application of whole heart segmentation, in future work we will consider to use local similarity measures to generate a best atlas for each local region.[15] The shape of the final atlas will be a fusion of all these locally best shapes via the proposed shape computation framework, where the transformations will be computed from the fused local velocities.

REFERENCES

[1] Davis, B. C., Fletcher, P. T., Bullitt, E., and Joshi, S., "Population Shape Regression From Random Design Data," in [*2007 IEEE 11th International Conference on Computer Vision*], 1–7, Ieee (2007).

[2] Rohlfing, T., Sullivan, E. V., and Pfefferbaum, A., "Regression models of atlas appearance.," in [*Information processing in medical imaging*], **21**, 151–62 (2009).

[3] Gerber, S., Tasdizen, T., Fletcher, P. T., Joshi, S., and Whitaker, R., "Manifold modeling for brain population analysis," *Medical image analysis* **14**(5), 643–53 (2010).

[4] Aljabar, P., Wolz, R., Srinivasan, L., Counsell, S., Boardman, J. P., Murgasova, M., Doria, V., Rutherford, M. A., Edwards, A. D., Hajnal, J. V., and Rueckert, D., "in a Manifold Learning Framework : Application to Neonatal MRI," in [*Medical Image Computing and Computer-Assisted Intervention*], 1–8 (2010).

[5] Cootes, T. F., Taylor, C. J., Cooper, D. H., and Graham, J., "Active shape models: Their training and application," *Computer Vision and Image Understanding* **61**, 38–59 (Jan 1995).

[6] Arsigny, V., Commowick, O., Pennec, X., and Ayache, N., "A log-euclidean framework for statistics on diffeomorphisms," in [*Medical image computing and computer-assisted intervention*], **9**, 924–31 (2006).

[7] Avants, B. and Gee, J., "Geodesic estimation for large deformation anatomical shape averaging and interpolation," *NeuroImage* **23**, S139–S150 (2004).

[8] Ashburner, J., "A fast diffeomorphic image registration algorithm," *NeuroImage* **38**, 95–113 (2007).

[9] Zhuang, X., Rhode, K., Razavi, R., Hawkes, D. J., and Ourselin, S., "A registration-based propagation framework for automatic whole heart segmentation of cardiac MRI," *IEEE Transactions on Medical Imaging* **29**(9), 1612–1625 (2010).

[10] Zhuang, X., Leung, K., Rhode, K., Razavi, R., Hawkes, D. J., and Ourselin, S., "Whole heart segmentation of cardiac MRI using multiple path propagation strategy," in [*Medical Image Computing and Computer Assisted Intervention (MICCAI'10).*], *Lecture Notes in Computer Science* **6361**, 435–443 (2010).

[11] Fletcher, P. T., Joshi, S., Ju, C., and Pizer, S. M., "Principal geodesic analysis for the study of nonlinear statistics of shape," *IEEE Transactions on Medical Imaging* **23**, 995–1005 (2004).

[12] Miller, M., "Computational anatomy: shape, growth, and atrophy comparison via diffeomorphisms," *NeuroImage* **23**, S19–S33 (2004).

[13] Beg, M. F., Miller, M. I., Trouvé, A., and Younes, L., "Computing Large Deformation Metric Mappings via Geodesic Flows of Diffeomorphisms," *International Journal of Computer Vision* **61**, 139–157 (Feb. 2005).

[14] Kittler, J., Hatef, M., Duin, R., and Matas, J., "On combining classifiers," *IEEE Transactions on Pattern Analysis and Machine Intelligence* **20**, 226–239 (1998).

[15] van Rikxoort, E., Isgum, I., Arzhaeva, Y., Staring, M., Klein, S., Viergever, M., Pluim, J., and van Ginneken, B., "Adaptive local multi-atlas segmentation application to the heart and the caudate nucleus," *Medical Image Analysis* (14), 39–49 (2010).